Journal of Catalysis 261 (2009) 17–22

Contents lists available at ScienceDirect

Journal of Catalysis

www.elsevier.com/locate/jcat

Understanding the nature of surface nitrates in BaO/γ-Al_2O_3 NO_x storage materials: A combined experimental and theoretical study

Ja Hun Kwak [a], Donghai Mei [a,*], Cheol-Woo Yi [a,1], Do Heui Kim [a], Charles H.F. Peden [a], Lawrence F. Allard [b], János Szanyi [a,*]

[a] Institute for Interfacial Catalysis, Pacific Northwest National Laboratory, P.O. Box 999, MSIN K8-80, Richland, WA 99352, USA
[b] High Temperature Materials Laboratory, Oak Ridge National Laboratory, TN, USA

ARTICLE INFO

Article history:
Received 20 June 2008
Revised 29 September 2008
Accepted 26 October 2008
Available online 22 November 2008

Keywords:
BaO/γ-Al_2O_3
NO_x storage
HR-STEM
FTIR
Density Functional Theory

ABSTRACT

A combined experimental-theory approach was applied to unambiguously determine the nature of "surface nitrates" in BaO/γ-Al_2O_3 NO_x storage materials. High resolution scanning transmission electron microscopy images reveal that at a low BaO coverage of 2 wt% on γ-Al_2O_3 monomeric BaO units are present almost exclusively. These molecularly dispersed BaO units are concentrated on the (100) facets of the alumina crystallites, while other facets remain practically BaO-free The results of the density functional theory calculations predicted adsorption geometries for the $(BaO)_x$ ($x = 1$ and 2) units. The energetically most favorable BaO monomer and dimer units anchor to pentacoordinate Al^{3+} sites on the (100) facets of γ-Al_2O_3 in such geometries that maximize their interactions with the support surface. The calculated vibrational frequencies of the energetically most favorable nitrate species formed upon the interaction of NO_2 with the monomeric and dimeric BaO units agree remarkably well with those observed experimentally by infrared spectroscopy and identified as "surface nitrates."

Published by Elsevier Inc.

1. Introduction

The special role of the interface between the active catalytic phase (metal or metal oxide) and the oxide support in determining the properties of practical catalysts has long been recognized [1]; however, it is still very poorly understood in most systems. The way the active phase is anchored onto the support surface may be especially important when the active phase is very highly dispersed. In such systems, the active oxide is likely anchored to some special sites of the support, and we may expect significant modifications in the chemical properties of these active centers by the underlying oxide support. Investigating the properties of these very highly dispersed active centers, however, is experimentally very difficult, and requires a concerted effort of both experimental and theoretical methods.

In recent years, BaO supported on γ-Al_2O_3 has attracted significant attention due to its potential application as a NO_x storage material used to treat exhaust emissions of internal combustion engines operating under lean (oxygen rich) conditions [2]. Numerous studies (both experimental and theoretical) have focused on the elucidation of the interaction of NO_2 with BaO, and the identification and characterization of NO_x species (nitrites and nitrates) formed on the BaO storage material and the γ-Al_2O_3 support as well. Density functional theory (DFT) calculations of both Schneider et al. [3–6] and Broqvist et al. [7] pointed to a pairwise, cooperative adsorption mechanism of NO_2 on BaO, resulting in the initial formation of nitrite–nitrate ion pairs. This initial cooperative NO_2 adsorption mechanism on pure BaO has recently been substantiated in an experimental study on model NO_x storage materials [8]. Very recently, we have reported the importance of a strong interaction between the BaO storage and alumina support materials in determining the adsorption mechanism of NO_2 [9]. Furthermore, the existence of two different types of nitrate species on BaO/γ-Al_2O_3-based NO_x storage/reduction systems has been evident in TPD, FTIR and ^{15}N solid state NMR studies [10]. Based on the results of these spectroscopic characterizations, we concluded that "surface" and "bulk" Ba-nitrate species formed when BaO/γ-Al_2O_3 NO_x storage materials were saturated with NO_2.

The nature of the bulk $Ba(NO_3)_2$ species on the γ-Al_2O_3 support is reasonably well understood, and its spectroscopic properties (IR vibrational frequencies of the nitrates) have been accurately predicted by DFT calculations [11,12]. On the other hand, no clear understanding has been developed on the nature of the so-called "surface nitrates."

In this contribution, we report the results of a combined experimental and DFT investigation in which we set out to understand the role of the interaction between BaO and γ-Al_2O_3 in the NO_2

* Corresponding authors. Fax: +1 509 371 6242.
E-mail addresses: donghai.mei@pnl.gov (D. Mei), janos.szanyi@pnl.gov (J. Szanyi).
[1] Present address: Department of Chemistry, Sungshin Women's University, Seoul, S. Korea.

0021-9517/$ – see front matter Published by Elsevier Inc.
doi:10.1016/j.jcat.2008.10.016

uptake process at low BaO loadings, and the characteristics of the "surface" nitrate species thus formed.

2. Experimental

The BaO/γ-Al_2O_3 NO_x storage materials with varying BaO loadings were prepared by traditional incipient wetness methods using a $Ba(NO_3)_2$ precursor, and a 200 m^2/g γ-Al_2O_3 support material from Condea. After drying the materials in air at 373 K, they were activated by calcination of 773 K in flowing dry air. The details of the IR measurements have been described in detail previously [10]. The HR-STEM images were obtained at the High Temperature Materials Laboratory located at Oak Ridge National Laboratory, using a JEOL 2200 FEF aberration corrected electron microscope.

We performed periodic DFT calculations using the Vienna ab initio simulation package (VASP) [13–16]. The projector augmented wave (PAW) method combined with a plane-wave basis and cutoff energy of 400 eV was used to describe core and valence electrons [17,18]. The Perdew–Burke–Ernzerhof (PBE) form of generalized gradient approximation (GGA) [19] was used in the calculations. The ground-state atomic geometries of NO_x/BaO/γ-Al_2O_3 systems were obtained by minimizing the forces on each atom to below 0.05 eV/Å. Spin-polarization was implemented in all calculations. The γ-Al_2O_3 bulk structure used in this work was taken from Digne et al.'s model [20]. The calculated lattice parameters of bulk γ-Al_2O_3 were $a = 5.58$ Å, $b = 8.41$ Å, $c = 8.07$ Å and $\beta = 90.53°$. These values are in good agreement with previous calculations [20,21]. As indicated in a recent experimental study [22], the Al^{3+}_{penta} sites could be the most active surface sites for anchoring deposited transition metal and metal oxide particles. Consequently, we focused on the γ-Al_2O_3(100) surface in this work because the Al^{3+}_{penta} sites are only available on the γ-Al_2O_3(100) surface.

The γ-Al_2O_3(100) surface was modeled as a 2×1 supercell using four atomic layers (11.16 Å × 8.41 Å × 8.37 Å). As shown in Fig. 2, the γ-Al_2O_3(100)-2×1 surface model consists of eight units of Al_2O_3 with only Al^{3+}_{penta} and tri-coordinated O^{2-} on the surface. The surface slab was symmetrical to avoid unphysical dipole–dipole interactions between the neighboring slabs. After testing different k-point grid schedules, a Monkhorst–Pack grid of size of $2 \times 2 \times 1$ was used to sample the surface Brillioun zone. The calculated surface energy is 960.6 mJ/m^2, which is consistent with previously reported values of 958 [21] and 970 [20] mJ/m^2.

Adsorption energies, $E^{ad}_{(BaO)_n}$, of BaO monomer or dimer on the γ-Al_2O_3(100) surface were calculated by Eq. (1)

$$E^{ad}_{(BaO)_n} = E_{(BaO)_n+\gamma\text{-}Al_2O_3(100)} - (E_{\gamma\text{-}Al_2O_3(100)} + E_{(BaO)_n}) \quad (1)$$

in which $E_{(BaO)_n+\gamma\text{-}Al_2O_3(100)}$ is the total energy of the interacting system of the γ-Al_2O_3(100) surface and $(BaO)_n$ ($n = 1$ or 2); $E_{\gamma\text{-}Al_2O_3(100)}$ is the total energy of the bare γ-Al_2O_3(100) surface; and $E_{(BaO)_n}$ is the energy of the isolated $(BaO)_n$ monomer or dimer in vacuum. Accordingly, the adsorption energies, $E^{ad}_{NO_2+NO_3}$, of co-adsorbed NO_2 + NO_3 pair on the γ-Al_2O_3(100) supported BaO monomer and dimer were calculated by Eq. (2)

$$E^{ad}_{NO_2+NO_3} = E_{NO_2+NO_3+(BaO)_n+\gamma\text{-}Al_2O_3} - (E_{(BaO)_n+\gamma\text{-}Al_2O_3} + E_{NO_2} + E_{NO_3}) \quad (2)$$

in which $E_{NO_2+NO_3+(BaO)_n+\gamma\text{-}Al_2O_3}$ is the total energy of co-adsorbed NO_2 + NO_3 pair on $(BaO)_n$ over the γ-Al_2O_3(100) surface; E_{NO_2} and E_{NO_3} are the energies of the isolated NO_2 and NO_3 molecules in the vacuum. For comparison, we also calculated the NO_2 + NO_3 pair adsorbed on the BaO(001) surface. This model was used to represent the bulk nitrate. The BaO(001) surface slab consists of a 2×2 super cell with three atomic layers. The same PAW-GGA and k-point sampling schedule for NO_x/BaO/γ-Al_2O_3 systems were used in the calculations of NO_x/BaO(001) system. The calculated surface energy of BaO(001) is 0.35 J/m^2. This is in good agreement with previous DFT results of 0.35 J/m^2 [3] with different functionals. In the same way, the adsorption energies, $E^{ad}_{NO_2+NO_3}$, of co-adsorbed NO_2 + NO_3 pair on the BaO(001) surface was calculated as follows

$$E^{ad}_{NO_2+NO_3} = E_{NO_2+NO_3+BaO(001)} - (E_{BaO(001)} + E_{NO_2} + E_{NO_3}) \quad (3)$$

in which $E_{NO_2+NO_3+BaO(001)}$ and $E_{BaO(001)}$ are the total energies of the NO_2 + NO_3 pair interacting with BaO(001) surface and the clean BaO(001) surface respectively. Based on above definitions, a negative $E^{ad}_{(BaO)_n}$ or $E^{ad}_{NO_2+NO_3}$ indicates a favorable (exothermic) adsorption.

3. Results and discussion

Fig. 1 shows a high resolution STEM image of a 2 wt% BaO/γ-Al_2O_3 sample. The image clearly shows that single BaO molecules (bright spots) are dispersed on the surface of γ-Al_2O_3. This high resolution TEM image allows us to differentiate regions on the γ-Al_2O_3 support that have significantly different BaO populations. In region A no BaO units are seen, in accord with the prediction of DFT calculations [20,21] that suggests the complete absence of pentacoordinate Al^{3+} (Al^{3+}_{penta}) sites on other facets that would serve as anchoring points for BaO. In regions B and C of the TEM image the BaO units are fairly uniformly dispersed, and as line sections 1 and 2 show they consist of single BaO units. The decoration of facet boundaries by BaO monomers seems to be also evident, for example in regions D of the HR-TEM image. These observations are all consistent with the results of our recent high resolution ^{27}Al solid state NMR study that showed the preferential anchoring of BaO monomers onto Al^{3+}_{penta} sites formed by the dehydroxylation of the γ-Al_2O_3(100) surface [22]. We have also shown that, in order to saturate all the Al^{3+}_{penta} sites on the γ-Al_2O_3 surface (with specific surface area of ~200 m^2/g) upon calcination at 773 K for 2 h, approximately 4 wt% BaO loading was required. This result suggests that at 2 wt% BaO loading about 50% of the Al^{3+}_{penta} sites are occupied by BaO monomers. When the BaO loading is increased to 8 wt%, the number of BaO molecules is twice that of the Al^{3+}_{penta} sites. Therefore, if we assume an even distribution of BaO on the γ-Al_2O_3 support surface, and that BaO only anchored to the γ-Al_2O_3 surface through Al^{3+}_{penta} sites, we may expect to observe two BaO molecules occupying each Al^{3+}_{penta} site. And, indeed, $(BaO)_2$ dimers dispersed on the γ-Al_2O_3 surface are the primary Ba-containing phase in the 8 wt% BaO/γ-Al_2O_3 sample, however, $(BaO)_x$ units with $x > 2$ present as well (TEM image not shown).

In order to characterize these $(BaO)_x$ ($x \leqslant 2$) units anchored to the Al^{3+}_{penta} sites on the γ-Al_2O_3 surface, and then their interactions with NO_2, we performed DFT calculations on these systems. As a model for the support material we have chosen a (2×1) unit cell of the γ-Al_2O_3(100) surface. Previous DFT calculations [23] have shown that this surface was completely dehydroxylated at 600 K; therefore, the effect of OH groups on the anchoring of $(BaO)_x$ units as well as on the NO_2 chemistry was not considered here. Fig. 2a shows the most stable structure of a BaO monomer anchored to a Al^{3+}_{penta} site on the γ-Al_2O_3(100) surface with an adsorption energy of −4.08 eV. The energetically most favorable configuration of the $(BaO)_2$ dimer on the dehydrated γ-Al_2O_3(100) surface is displayed in Fig. 2b. The adsorption energy of this $(BaO)_2$ dimer is −3.82 eV, slightly lower than that found for the BaO monomer. These model calculations show that both the BaO monomer and the $(BaO)_2$ dimer assume configurations on the γ-Al_2O_3(100) surface that maximize their interactions with the support material; i.e. the Ba–O bond is almost parallel with the support surface.

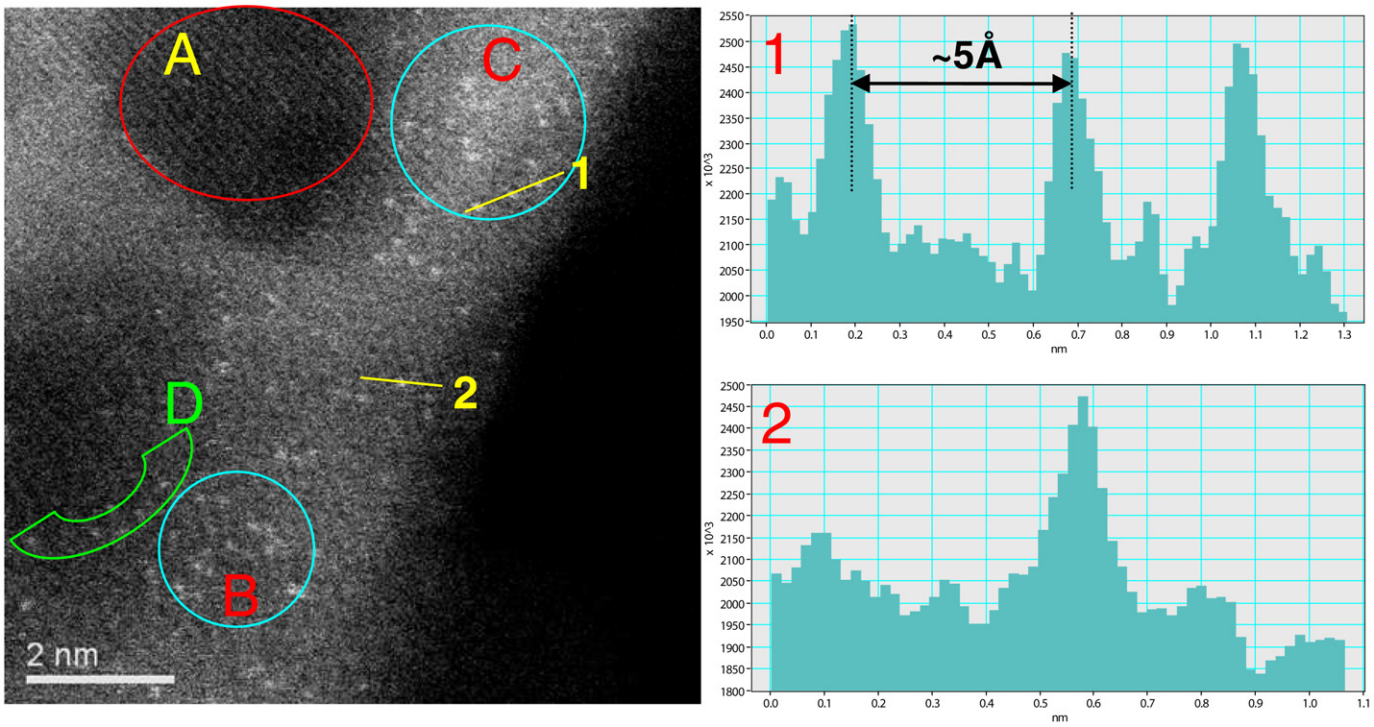

Fig. 1. HR-STEM image of a 2 wt% BaO/γ-Al_2O_3 sample. Normalized intensities across BaO monomers at two different regions of the image are also shown (1 and 2).

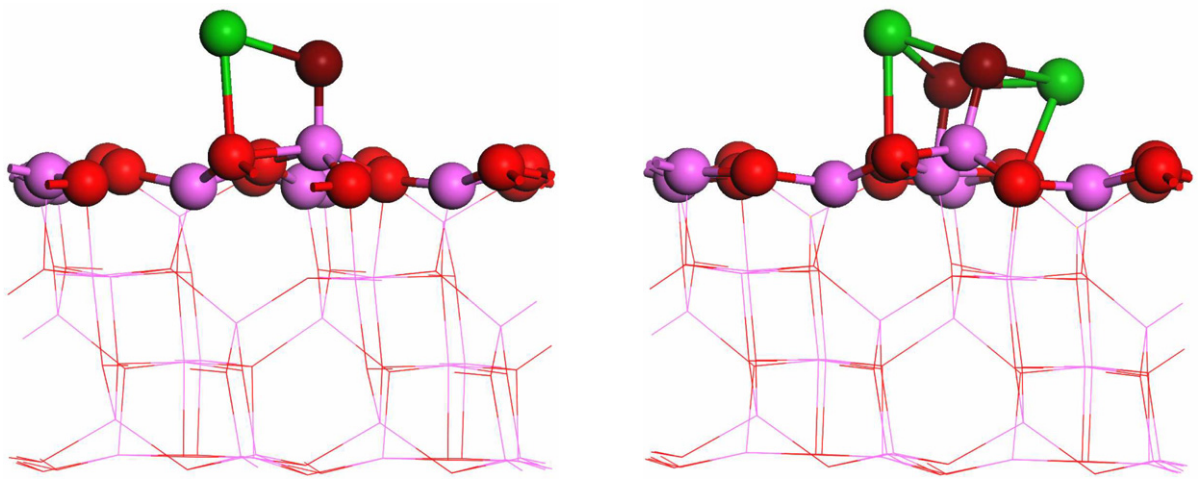

(a) (b)

Fig. 2. Structures of a BaO monomer (a) and dimer (b) on a dehydroxylated γ-Al_2O_3(100) surface (green: Ba; dark red: O in BaO; magenta: Al^{3+}_{penta} and red: surface O atom on the γ-Al_2O_3(100) surface; bulk alumina indicated by the light lines.

These geometries allow the O^{2-} ion of BaO to interact with the coordinatively unsaturated Al^{3+}_{penta} ion, while the Ba^{2+} ion binds with surface oxygens of the γ-Al_2O_3 support. An analysis of Bader charge distributions [24,25] on the adsorbed $(BaO)_x$ ($x = 1$ or 2) species indicates that the Bader charges of the Ba^{2+} and O^{2-} ions on the alumina surface are almost the same as the corresponding charges of Ba and O ions in bulk BaO and on the BaO(001) surface. The adsorption of these BaO units on the fully dehydrated γ-Al_2O_3(100) surface, however, results in significant surface and adsorbate relaxations, reflected by the large changes to metal ion–oxygen ion distances for both the adsorbed BaO and the alumina surface. For example, the Ba–O bond length increased from 2.05 Å in the free BaO monomer to 2.37 Å in the adsorbed BaO monomer; similar changes were seen in the $(BaO)_2$ dimer as well. The surface deformation energy (i.e. the surface energy difference between the clean and the $(BaO)_x$-modified γ-Al_2O_3(100) surfaces) for the energetically most favorable adsorption complexes were calculated to be 3.20 eV for the γ-Al_2O_3(100) surface accommodating BaO monomers, and 5.33 eV for the one with $(BaO)_2$ dimer. These changes in the surface energy further indicate adsorbate-induced rearrangements on the γ-Al_2O_3(100) surface that are materialized in the elongation of the Al–O bonds participating in the formation of the adsorption complexes (see Table 1).

Now that we have clarified the structures of $(BaO)_x$ ($x = 1$ or 2) units that form on the γ-Al_2O_3(100) surface at low BaO coverages, we will focus on the interactions of BaO monomers and dimers with NO_2, and the characterization of the NO_x species formed. Although, in practical NO_x storage systems the BaO loading is usually at or above 20 wt%, here we concentrate on BaO/γ-Al_2O_3 materials with low BaO loadings in order to avoid the formation of large

Table 1
The adsorption energies (eV/BaO) and structural parameters (Å) of BaO monomer and dimer on the γ-Al_2O_3(100) surface.

Adsorbate	Adsorption energy	Bond length		
		d(Ba–O_{surf})	d(O–Al_{surf})	d(Ba–O)
BaO	−4.08	2.66; 2.77	1.74	2.37
$(BaO)_2$	−3.82	2.59; 2.66	1.79; 1.85	2.33; 2.41; 2.42; 2.76

BaO particles that would lead to the formation of bulk $Ba(NO_3)_2$ upon NO_2 exposure.

Six nitrate models formed by NO_2 interacting with $(BaO)_x$/γ-Al_2O_3 and BaO(001) surfaces were examined. The energetics and structural parameters are given in Table 2. The optimized structures of nitrates on a BaO monomer over the γ-Al_2O_3(100) surface are shown in Fig. 3a. In this configuration (model I in Table 3), NO_3 is bonded to the Ba ion in a bidentate configuration and NO_2 is bonded to an O ion via the N-atom. The calculated vibrational frequency for the asymmetric stretch of NO_2–O_{BaO} is 1600 cm^{-1}, while the in-plane bending mode for the same species is at 1275 cm^{-1}. The frequencies of these modes for the NO_3^-–Ba species are predicted at 1545 and 1207 cm^{-1}, respectively. The higher frequency bands of these nitrate vibrations agree well with those measured in FTIR experiments (see below); i.e. between 1550 and 1600 cm^{-1}. However, the calculated lower frequency bands are at somewhat lower wavenumbers than those determined experimentally.

We have also calculated the frequencies of the various nitrate vibrations for model (II) illustrated in Fig. 3b, where the BaO monomer-bound nitrates are allowed to interact with the alumina surface (oxygen atoms in the nitrate ion interact with neighboring Al^{3+}_{penta} sites). In fact, our calculations show that this configuration of the nitrate species on the BaO monomer (Fig. 3b) is energetically more stable by 0.46 eV. The calculated vibrational frequencies of these Ba-bound nitrates are somewhat higher than those ones where the alumina-nitrate interaction was not considered. The asymmetric NO_3^-–Ba vibrational stretch modes for this structure are calculated at 1574 and 1237 cm^{-1}, the asymmetric NO_2–O_{BaO} mode at 1565 cm^{-1} and the in-plane bending mode of NO_2–O_{BaO} at 1232 cm^{-1}. The higher frequency vibrations match perfectly the ones determined by experiments, but the lower frequency ones are still somewhat lower.

We also examined the nitrate structures formed by NO_x adsorption on the $(BaO)_2$ dimer-covered γ-Al_2O_3(100) surface. The calculated vibrational frequencies of the most stable structures (model III and IV) are listed in Table 3. Compared with the results for nitrate–BaO monomer complexes, we notice that the higher vibrational frequencies of nitrate–$(BaO)_2$ are redshifted. On the other hand, the two lower frequencies are blueshifted at 1302 and 1256 cm^{-1} for the model IV configuration, making them quite close to experimentally measured values. The model IV structure is found to be thermodynamically more stable than model III by 0.89 eV.

In order to validate our vibrational frequency calculations, we also calculated the positions of nitrate vibrational features in a structure where nitrates were formed on the (001) surface of bulk BaO. This allows us to directly compare our DFT predictions with those of both previous theoretical calculations [11,12] and experiments [10,11,26–32]. We calculated the nitrate vibrational frequencies for two models (V and VI): the one proposed by Grönbeck et al. [7], and the other used by Schneider et al. [3]. The results of these calculations, together with those obtained for the BaO monomer- and dimer-bound nitrates on the γ-Al_2O_3(100) surface (discussed above), are summarized in Table 3. The predicted frequencies of nitrite–nitrate pair on the BaO(001) surface from our calculations are very close to those calculated by Broqvist et al. [11] with a $(BaO)_9$ cluster model representing BaO(001) surface, and consistent with the experimental results measured for

Table 2
The adsorption energies (eV) and structural parameters (Å) of the NO_2 + NO_3 pair on different surfaces.

Model	Surface	Adsorption energy	Structural parameters				
			d(NO_2–O_{BaO})	d(NO_3–Ba)	d(NO_2–O_{surf})	d(NO_3–Al_{surf})	d(NO_2–Al_{surf})
I	BaO/γ-Al_2O_3(100)	−3.67	1.37	2.62, 2.64			
II	BaO/γ-Al_2O_3(100)	−4.13	1.27	2.67, 2.75	2.05	2.10	
III	$(BaO)_2$/γ-Al_2O_3(100)	−4.75	1.30	2.62, 2.66			2.08
IV	$(BaO)_2$/γ-Al_2O_3(100)	−5.64	1.27	2.89, 3.09			2.05
			d(NO_2–O_{surf})	d(NO_3–O_{surf})	d(NO_3–Ba_{surf})		
V	BaO(001)	−4.24	1.33	2.80			
VI	BaO(001)	−3.81	1.33		2.71		

Table 3
Comparison of calculated vibrational frequencies of nitrates (bound to a BaO monomer, a BaO dimer, and to BaO(001) surface) with experimentally measured ones.

Mode of vibration	Model						Broqvist et al. [11]	Exp. [10]
	I	II	III	IV	V	VI		
	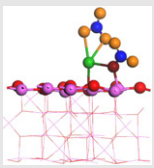	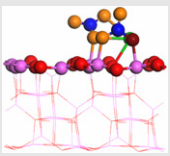	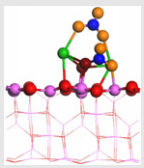	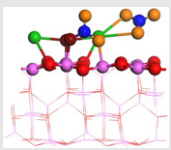	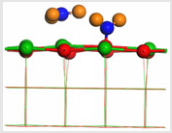	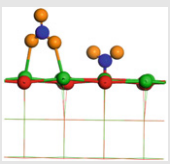		
Asym. NO_2–O_{BaO}	1600	1565	1544	1572	1450	1443	1448	Surface nitrate:
Asym. NO_3–Ba	1545	1574	1506	1529	1409	1476	1460	1574–1620
In-plane bending NO_2–O_{BaO}	1275	1232	1206	1302	1240	1235	1228	1234–1320
In-plane bending NO_3–Ba	1207	1237	1249	1256	1318	1261	1278	
Sym. NO_3–Ba	1010	971	1044	1017	1016	1047		Bulk nitrate:
Sym. NO_2–O_{BaO}	902	981	1014	1033	912	898		1420–1480

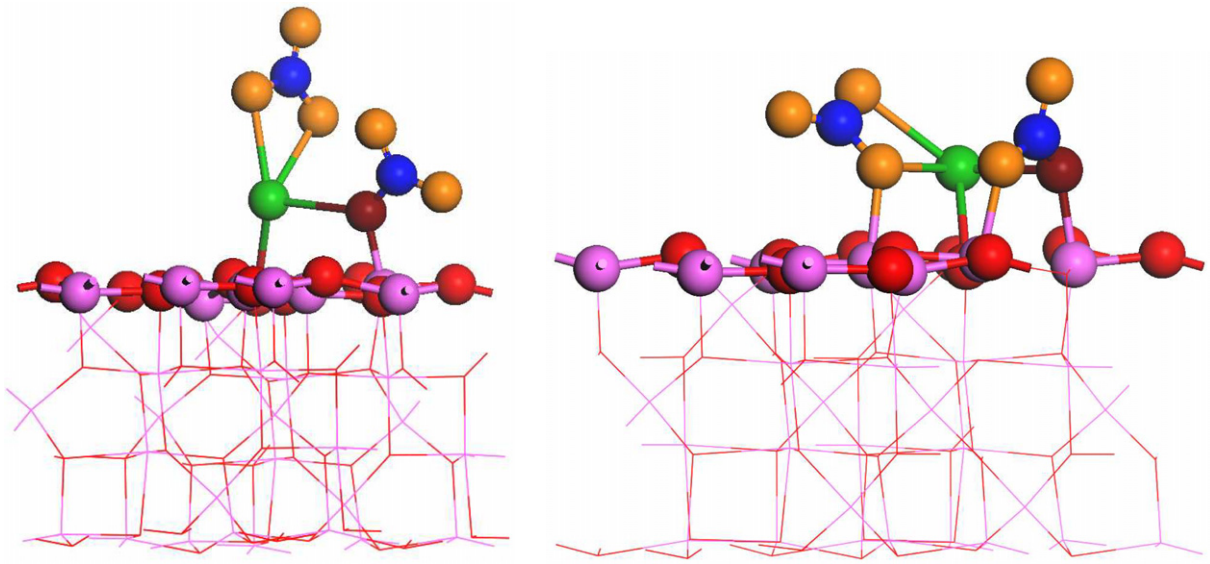

(a) (b)

Fig. 3. Optimized structures of $Ba(NO_3)_2$ monomers on the γ-Al_2O_3(100) surface: (a) nitrates did not interact with the γ-Al_2O_3(100) surface; and (b) γ-Al_2O_3(100) surface mediated (blue: N; gold: O in NO_x; green: Ba; dark red: O in BaO; magenta: Al^{3+}_{penta}; and red: O atoms on the γ-Al_2O_3(100) surface).

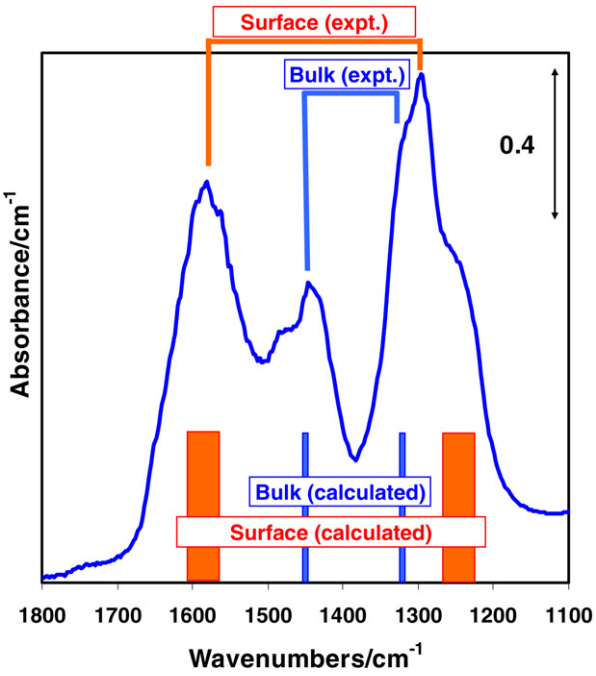

Fig. 4. FTIR spectrum obtained from an 8 wt% BaO/γ-Al_2O_3 sample after NO_2 saturation at 300 K. The calculated IR vibrational frequencies for the nitrate species formed are displayed as well.

bulk $Ba(NO_3)_2$ species on alumina support materials [10]. An IR spectrum recorded from an 8 wt% BaO/γ-Al_2O_3 after saturation with NO_2 at 300 K (both surface and bulk nitrates are present) is shown in Fig. 4, together with the vibrational frequency ranges our calculation predicted for nitrates bound to $(BaO)_x$ on the γ-Al_2O_3 (red columns) and BaO(100) (blue columns). The agreement between the experimentally measured frequencies and DFT predictions for both "surface" and "bulk" BaO-bound nitrates is excellent. This clearly indicates the existence of two different forms of nitrates on the alumina supported BaO NO_x storage material. (The calculated absolute frequency values for the nitrates associated with $(BaO)_x$ ($x \leqslant 2$) may not match perfectly the experimentally measured ones, however, they clearly show the fundamental differences between nitrates associated with bulk and surface $Ba(NO_3)_2$ species. The absolute frequency values of the surface nitrates are probably influenced by other factors than the $(BaO)_x$ cluster size and the interaction with the alumina support, like the presence and concentration of surface hydroxyl groups.)

All previous theoretical calculations reported to date have focused on the reaction of NO_x (mostly NO_2) with pure, unsupported alkaline earth oxides (especially the (100) surface of crystalline BaO, and $(BaO)_x$ ($x \leqslant 12$) clusters as models of bulk BaO) [3–7,11]. As we have mentioned above, these calculations provided valuable insight into the NO_x uptake mechanism on pure BaO and predicted, with good accuracy, the vibrational spectroscopic properties of the nitrate species thus formed. However, they ignored the possible role of the interaction between BaO and γ-Al_2O_3 on the NO_2 uptake mechanism, and the properties of the nitrates that formed on supported BaO. The results of our surface science studies on model NO_x storage materials (BaO/Al_2O_3/NiAl(110)) [8,9] have clearly demonstrated that very different NO_2 uptake mechanisms operate on pure BaO (high BaO loading), and at the BaO/Al_2O_3 interface (low BaO loading). These preceding studies also confirmed the importance of the strong interaction between BaO and Al_2O_3 on both the NO_2 uptake mechanism, and the characteristics of the NO_x species formed. The results of our current study, in conjunction with our prior work on both model and supported BaO/γ-Al_2O_3 NO_x storage systems, allows the unambiguous identification of the different nitrate species that we earlier identified as "surface" and "bulk" nitrates. Bulk nitrates can be envisioned as nitrates formed on the surfaces and in the bulk of BaO particles, while surface nitrates are the ones that form on alumina-supported $(BaO)_x$ species (monomers, dimers, and/or possibly small clusters with somewhat higher x values) that are bound to Al^{3+}_{penta} sites. The properties of these very small $(BaO)_x$ units are fundamentally different from those of the bulk BaO particles. Their strong interaction with the alumina surface alters their chemical properties in their reaction with NO_2, thus altering their spectroscopic characteristics.

4. Conclusion

This combined experimental and theoretical study clearly illustrates the power of such a concerted effort to unravel the interactions of NO_x molecules with oxide (mixed oxide) surfaces. The results of these combined studies have allowed us to develop a clear understanding of the nature of both the surface and bulk types of nitrates on the BaO/γ-Al_2O_3 NO_x storage system, a subject actively debated in the literature for some time. Surface nitrates are associated with $(BaO)_x$ units where $x \leqslant 2$, while bulk nitrates represent those formed by the interaction of NO_2 with bulk BaO. The properties of surface Ba-nitrates are strongly influenced by their interactions with the alumina support. Furthermore, this study has implications for understanding the properties of alumina-supported metal and metal-oxide catalysts when the active phases are present at low loadings (i.e., high dispersions).

Acknowledgments

We gratefully acknowledge the US Department of Energy (DOE), Office of Basic Energy Sciences, Division of Chemical Sciences for the support of this work. The research described in this paper was performed at the Environmental Molecular Sciences Laboratory (EMSL), a national scientific user facility sponsored by the DOE Office of Biological and Environmental Research and located at Pacific Northwest National Laboratory (PNNL). PNNL is operated for the US DOE by Battelle Memorial Institute under contract number DE-AC05-76RL01830. This work also supported by the LDRD project of Catalysis Initiative at PNNL. The computing time was granted by National Energy Research Scientific Center (NERSC). We also acknowledge the High Temperature Materials Laboratory at ORNL where the HR-STEM images were acquired.

References

[1] A.Y. Stakheev, L.M. Kustov, Appl. Catal. A 188 (1999) 3.
[2] N. Takahashi, H. Shinjoh, T. Iijima, T. Suzuki, K. Yamazaki, K. Yokota, H. Suzuki, N. Miyoshi, S. Matsumoto, T. Tanizawa, T. Tanaka, K. Sasahara, Catal. Today 27 (1996) 63.
[3] W.F. Schneider, J. Phys. Chem. B 108 (2004) 273.
[4] M. Miletic, J.L. Gland, K.C. Hass, W.F. Schneider, Surf. Sci. 546 (2003) 75.
[5] M. Miletic, J.L. Gland, K.C. Hass, W.F. Schneider, J. Phys. Chem. B 107 (2003) 157.
[6] W.F. Schneider, K.C. Hass, M. Miletic, J.L. Gland, J. Phys. Chem. B 106 (2002) 7405.
[7] H. Grönbeck, P. Broqvist, I. Panas, Surf. Sci. 600 (2006) 403.
[8] C.W. Yi, J.H. Kwak, J. Szanyi, J. Phys. Chem. C 111 (2007) 15299.
[9] C.W. Yi, J.H. Kwak, C.H.F. Peden, C. Wang, J. Szanyi, J. Phys. Chem. C 111 (2007) 14942.
[10] J. Szanyi, J.H. Kwak, D.H. Kim, S.D. Burton, C.H.F. Peden, J. Phys. Chem. B 109 (2005) 27.
[11] P. Broqvist, H. Grönbeck, E. Fridell, E.I. Panas, J. Phys. Chem. B 108 (2004) 3523.
[12] A. Desikusumatsuti, T. Staudt, H. Grönbeck, J. Libuda, J. Catal. 255 (2008) 127.
[13] G. Kresse, J. Hafner, Phys. Rev. B 47 (1993) 558.
[14] G. Kresse, J. Hafner, Phys. Rev. B 49 (1994) 14251.
[15] G. Kresse, J. Furthmuller, Comput. Mater. Sci. 6 (1996) 15.
[16] G. Kresse, J. Furthmuller, Phys. Rev. B 54 (1996) 11169.
[17] P.E. Blochl, Phys. Rev. B 50 (1994) 17953.
[18] G. Kresse, D. Joubert, Phys. Rev. B 59 (1999) 1758.
[19] J.P. Perdew, K. Burke, M. Ernzerhof, Phys. Rev. Lett. 77 (1996) 3865.
[20] M. Digne, P. Sautet, P. Raybaud, P. Euzen, H. Toulhoat, J. Catal. 226 (2004) 54.
[21] S. Kim, D.C. Sorescu, O. Byl, J.T. Yates Jr., J. Phys. Chem. B 110 (2006) 4742.
[22] J.H. Kwak, J.Z. Hu, D.H. Kim, J. Szanyi, C.H.F. Peden, J. Catal. 251 (2007) 189.
[23] M. Digne, P. Sautet, P. Raybaud, P. Euzen, H. Toulhoat, J. Catal. 211 (2002) 1.
[24] R.F.W. Bader, Acc. Chem. Res. 18 (1985) 9.
[25] G. Henkelman, A. Arnaldsson, H. Jonsson, Comput. Mater. Sci. 36 (2006) 354.
[26] B. Westerberg, E. Fridell, J. Mol. Catal. 165 (2001) 249.
[27] F. Prinetto, G. Ghiotti, I. Nova, L. Lietti, E. Tronconi, P. Forzatti, J. Phys. Chem. B 105 (2001) 12732.
[28] I. Nova, L. Castoldi, L. Lietti, E. Tronconi, P. Forzatti, F. Prinetto, G. Ghiotti, J. Catal. 222 (2004) 377.
[29] Ch. Hess, J.H. Lunsford, J. Phys. Chem. B 106 (2002) 6358.
[30] P.T. Fanson, M.R. Horton, W.N. Delgass, J. Lauterbach, Appl. Catal. B 46 (2004) 393.
[31] N.W. Cant, M.J. Patterson, Catal. Today 73 (2002) 271.
[32] J.A. Anderson, A.J. Patterson, M. Fernandez-Garcia, in: A. Corma, F.V. Melo, S. Mendioroz, J.L.G. Fierro (Eds.), Stud. Surf. Sci. Catal., vol. 130, 2000, p. 1331.